

Simplified description of self-pulsation and excitability by thermal and free-carrier effects in semiconductor microcavities

Thomas Van Vaerenbergh,^{1,2,*} Martin Fiers,^{1,2} Joni Dambre,³ and Peter Bienstman^{1,2}

¹*Photonics Research Group, INTEC, Ghent University-imec, Sint-Pietersnieuwstraat 41, B-9000 Ghent, Belgium*

²*Center for Nano- and Biophotonics, Ghent University, Sint-Pietersnieuwstraat 41, B-9000 Ghent, Belgium*

³*Electronics and Information Systems, Ghent University, Sint-Pietersnieuwstraat 41, B-9000 Ghent, Belgium*

(Received 3 September 2012; published 5 December 2012)

Silicon-on-insulator microrings both self-pulsate and are excitable due to the presence of thermal and free-carrier-related nonlinearities. We show how a dimensionless mean-field model, in which the fast light dynamics are neglected and only the temperature and the amount of free carriers remain as variables, can explain this dynamic behavior. Apart from a scaled detuning of the input wavelength to the resonance wavelength and a scaled input power, this system contains only a limited number of dimensionless parameters dependent on both the geometry and material system of the cavity. Moreover, the onset of oscillation is still analytically tractable, while the excitability onset can be obtained using continuation algorithms. In agreement with previous experiments, excitability is predicted to appear mainly at the blue side of the resonance. Finally, the proposed method of analysis paves the way for an easy comparison of the dynamics in different material systems or cavity types.

DOI: [10.1103/PhysRevA.86.063808](https://doi.org/10.1103/PhysRevA.86.063808)

PACS number(s): 42.65.Sf, 42.79.Ta, 42.82.Et, 42.15.Eq

I. INTRODUCTION

A high Q/V ratio enhances light-matter interaction in a microcavity and accordingly reduces the required input power for nonlinear behavior. Consequently, in a passive microcavity with a high Q/V ratio, if the resonance wavelength of light with sufficiently high input power is detuned close to the resonance wavelength of the cavity, both self-pulsation and excitability can be observed [1–6].

In silicon-on-insulator (SOI) cavities, two-photon absorption (TPA) generates both free carriers and heat. Other heating mechanisms are surface-state absorption (SSA) and free-carrier absorption (FCA). The presence of the free carriers induces a blueshift of the resonance wavelength, known as free-carrier dispersion (FCD), while the heating of the cavity induces a redshift due to the thermo-optic effect. The difference between the time scales of the fast free-carrier dynamics and the slow heating effects results in self-pulsation in whispering-gallery-mode cavities such as microdisks and microrings [1–4]. In InP-based two-dimensional (2D) photonic crystal (PhC) resonators or PhC nanocavities a similar type of self-pulsation is visible [5,6], even though the main heating and free-carrier generation mechanism in this material system is single-photon absorption (SPA) instead of TPA. Moreover, close to the self-pulsation region excitability is perceived both in InP PhC cavities and SOI microrings, mainly at the blue side of the resonance [4–6].

This dynamic behavior can be described accurately using mean-field models, such as temporal coupled-mode theory [2–4]. In a unidirectional microring or microdisk (i.e., if backscattering is neglected) or a unimodal PhC cavity we represent the light in the cavity by a complex amplitude a and incorporate both the temperature difference of the cavity with the surroundings ΔT and the amount of free carriers N as two additional dynamic variables. This model allows us to calculate

realistic steady-state curves, and from linear stability analysis the oscillation onset can be identified as an Andronov-Hopf bifurcation [3,4]. Moreover, phase-plane analysis illustrates that the self-pulsation is caused by the interplay between temperature and free-carrier effects, indicating that the fast light dynamics are less relevant [4,6]. Using bifurcation diagrams, it can be shown that the excitability in a SOI microring appears near a subcritical Andronov-Hopf bifurcation [4]. However, a thorough analysis of the influence of the cavity design and different material parameters on the oscillation and excitability onset is still missing, as it is not straightforward to analyze this four-dimensional system (consisting of one complex variable a and two real variables ΔT and N) and the influence of its many parameters in a systematic manner.

Therefore, several simplified models have been proposed. For instance, recent publications show how, in nonlinear cavities in which the (slow) thermal heating effects are neglected, bistability, self-pulsation, and even chaos can appear, provided the remaining cavity nonlinearities (e.g., the free-carrier effects) have a sufficiently fast relaxation time compared to the photon lifetime [7–9]. Of course, due to the absence of heating effects, this self-pulsation is caused by physical mechanisms other than the one discussed in this paper. Importantly, bifurcation diagrams of the onset of bistability and self-pulsation can be calculated for the reduced models of those cavities.

In this paper, we show how a similar calculation method can be applied on a simplified model that, besides the free-carrier nonlinearities, does incorporate the thermal heating effects. For this purpose, we start from the equations of motion proposed in [4] and adiabatically eliminate the fast light dynamics (buildup time of the cavity light), so we end up with a 2D system. The remaining dynamic variables represent ΔT and N , respectively. This dimensionality reduction allows the semianalytic calculation of bifurcation diagrams of the simplified system. We use this calculation, e.g., to explain why excitability has until now been observed mainly at the blue

*thomas.vanvaerenbergh@intec.ugent.be

side of the resonance. For the analysis of the excitability onset we use PYDSTOOL [10] to continue the limit cycles, while the time traces are calculated with our in-house nonlinear circuit simulator CAPHE [11,12].

II. MATHEMATICAL MODEL

In this section, we derive the equations of motion of the cavity. Throughout this paper, we use the same parameter values as in [4], representing a typical critically coupled all-pass SOI microring with self-pulsing behavior, unless otherwise mentioned. However, we emphasize that the proposed approach is also usable for other material systems and cavity types. First, we rescale both ΔT and N to a dimensionless variable:

$$\Theta = \frac{2Q}{n_g} \frac{dn}{dT} \Delta T, \quad n = \frac{2Q}{n_g} \left| \frac{dn}{dN} \right| N. \quad (1)$$

Here, $dn/dT > 0$ is the thermal index change, $dn/dN < 0$ is the free-carrier index change, and n_g is the group index. As $\delta = (\omega - \omega_r)\tau_{ph}$ is the (normalized) detuning of the input light to the resonance frequency ω_r of a cavity with photon lifetime τ_{ph} (and thus $Q = \omega_r\tau_{ph}/2$), Θ and n can be interpreted as the absolute value of the (normalized) induced detuning shift caused by ΔT and N , respectively.

In SOI, the influence of TPA is at least one or two orders of magnitude smaller than the other nonlinear effects. If we neglect this influence, both on the broadening of the resonance width and the heating of the cavity, the equations of motion of the optical field a in the cavity and these nonlinear detunings Θ and n become [2–4]

$$\frac{da}{dt} = \frac{1}{\tau_{ph}} [j(-\delta - \Theta + n) - (1 + fn)]a + j \sqrt{\frac{2}{1+k}} \frac{P_{in}}{\tau_{ph}}, \quad (2)$$

$$\frac{d\Theta}{dt} = \frac{1}{\tau_{th}} \left[-\Theta + \frac{|a|^2}{P_0^{th} \tau_{ph}} (1 + efn) \right], \quad (3)$$

$$\frac{dn}{dt} = \frac{1}{\tau_{fc}} \left[-n + \frac{|a|^4}{(P_0^{el} \tau_{ph})^2} \right], \quad (4)$$

where we introduced the thermal and electric characteristic intrinsic power of the cavity [13]:

$$P_0^{th} = \frac{\rho_{Si} c_{p,Si}}{4 \frac{dn}{dT} \tau_{th} \eta_{lin} \Gamma_{th}} \frac{V_{th}}{Q_i} \left(\frac{1+k}{k} \right)^2, \quad (5)$$

$$P_0^{el} = \sqrt{\frac{\hbar \omega_r^3}{4 \left| \frac{dn}{dN} \right| \tau_{fc} \Gamma_{FCA} \beta_{Si} V_g^2}} \frac{V_{FCA}}{Q_i^{3/2}} \left(\frac{1+k}{k} \right)^{3/2}. \quad (6)$$

Here, τ_{th} and τ_{fc} are the relaxation times for the temperature and the free carriers, respectively. β_{Si} is the constant governing TPA, $c_{p,Si}$ is the thermal capacity, ρ_{Si} is the density of silicon, and n_g is the group index. We also use the effective volumes V_α and confinements Γ_α corresponding to a physical effect α , defined in [3,14]. η_{lin} is the fraction of the linear loss due to absorption (≈ 0.4 in SOI [1,14]). $Q_i = \frac{\omega_r \tau_i}{2}$ is the intrinsic Q factor of this cavity. Similar to [14], $k = \frac{\tau_c}{\tau_i}$ is the ratio of “good” loading (lifetime τ_c) to the parasitic and intrinsic loss channels (lifetime τ_i) of the resonator. The loaded Q factor of the cavity is then $Q = Q_i k / (1+k)$. For a critically coupled

cavity $k = 1$, for an undercoupled cavity $k > 1$, and for an overcoupled cavity $k < 1$. In Eqs. (2) and (3),

$$f = \frac{\frac{\sigma_{Si} c}{n_g}}{2 \frac{\omega_r}{n_g} \frac{dn}{dN}} \quad (7)$$

is the ratio of the broadening of the resonance width due to FCA (σ_{Si} is the absorption cross section of FCA) to the shift of the resonance peak due to FCD. Finally, $e = \frac{1+k}{k\eta_{lin}}$, while ef represents the additional heating due to FCA. By putting $\frac{da}{dt} = 0$ in Eq. (2), the steady-state value of the optical energy in the cavity, normalized to $\sqrt{P_0^{th} \tau_{ph}}$ ($a' = a / \sqrt{P_0^{th} \tau_{ph}}$), can be calculated:

$$|a'_{ss}|^2 = \frac{p}{(1 + fn)^2 + (\delta + \Theta - n)^2}, \quad (8)$$

where $p = P_{in} / (P_0^{th} \frac{1+k}{2})$ is the normalized version of the input power. As τ_{ph} is considerably smaller than τ_{fc} and τ_{th} , we do an adiabatic elimination of the optical field; i.e., for a given $\Theta(t)$ and $n(t)$, we approximate $|a'|^2(t)$ with its “steady-state” value $|a'_{ss}|^2$. Expressing time τ in units τ_{th} ($\tau = t / \tau_{th}$), the equations of motion of (Θ, n) are then

$$\frac{d\Theta}{d\tau} = -\Theta + \frac{p(1 + efn)}{(1 + fn)^2 + (\delta + \Theta - n)^2}, \quad (9)$$

$$\frac{dn}{d\tau} = \frac{1}{\epsilon} \left[-n + \left(\frac{pq}{(1 + fn)^2 + (\delta + \Theta - n)^2} \right)^2 \right]. \quad (10)$$

In these equations, $\epsilon = \tau_{fc} / \tau_{th}$, while $q = \frac{P_0^{th}}{P_0^{el}}$ determines the relative importance of the thermo-optic effect versus FCD. If FCD is absent, $q = 0$ (as $P_0^{el} = \infty$), while if the thermo-optic effect is absent $q = \infty$ (as $P_0^{th} = \infty$). Therefore, a relatively strong FCD corresponds to a large q value. For the convenience of the reader, we summarize the previous model parameters, together with their formulas and a short description of their meaning, in the Appendix.

These simplified equations still incorporate both self-pulsation (Fig. 1, top) and excitability (Fig. 1, bottom). In the rest of this paper, unless otherwise mentioned, we use $q = 0.397$, $\epsilon = 0.0815$, $f = 0.0714$, and $e = 5$ as ring parameters. P_{out} is calculated based on Eq. (8), and power is normalized to $(P_0^{th} \frac{1+k}{2})$.

Similar to [4], a phase-plane analysis of the time traces is useful to explain the dynamics of the system (Fig. 2). The time traces from Fig. 1 follow the direction changes indicated by the nullclines ($d\Theta/d\tau = 0, dn/d\tau = 0$). Moreover, the rectangular-like pulse shape of both the self-pulsation and excitation pulses is caused by fast relaxations ($\sim \tau_{fc}$) of the trajectory towards the $dn/d\tau = 0$ nullcline, alternating with a period in which the trajectory slowly ($\sim \tau_{th}$) follows this nullcline.

III. INFLUENCE OF CAVITY DESIGN ON NONLINEARITY ENHANCEMENT

The cavity design enhances the input power for the different physical effects with different scaling laws of the design parameters of the cavity (Q_i, V, k, \dots). In other words, for a given P_{in} , a good choice of (Q_i, V, k, \dots) can optimize p (SSA-induced heating), ep (FCA-induced heating), and/or qp (free-carrier generation). Therefore, in this section, we study

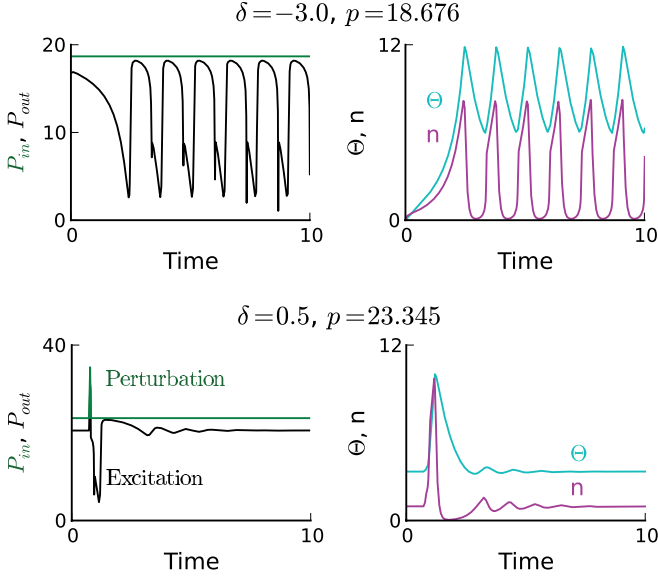


FIG. 1. (Color online) At $\delta = -3$ and $p = 18.676$ the microring self-pulsates, while at $\delta = 0.5$ and $p = 23.345$ the ring is excitable: a sufficiently strong perturbation can trigger a pulse. Ring parameters are $q = 0.397$, $\epsilon = 0.0815$, $f = 0.0714$, and $e = 5$. Simulations are done with CAPHE.

how the cavity design can affect the values of model parameters p , q , and e (Table I summarizes some relevant definitions).

A. Influence of Q_i and k on p , ep and qp

From Eq. (5) we obtain $P_0^{\text{th}} \propto \frac{1}{\eta_{\text{lin}}} \frac{V}{Q_i} \left(\frac{1+k}{k}\right)^2$, and consequently, $p \propto (2\eta_{\text{lin}} \frac{k^2}{(1+k)^3}) \frac{Q_i}{V} P_{\text{in}}$. This proportionality ex-

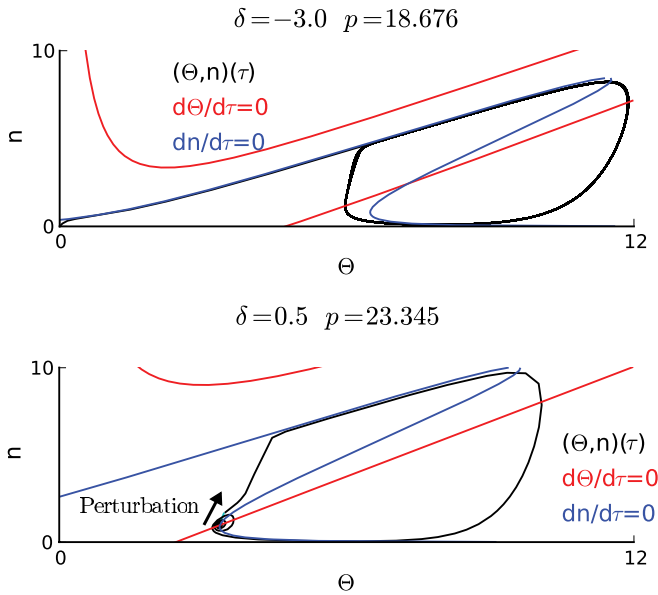


FIG. 2. (Color online) In the phase plane, the signal makes, both (top) for the self-pulsation time trace ($\delta = -3$ and $p = 18.676$) and (bottom) for the excitability time trace ($\delta = 0.5$ and $p = 23.345$) from Fig 1, a fast transition between the upper and lower branches of the $dn/d\tau = 0$ nullcline, while in between these transitions it slowly follows those branches.

presses how the cavity enhances the thermal nonlinearity for a given input power P_{in} . Given the cavity losses, the optimization of the light coupling into the cavity (i.e., k) can enhance the nonlinearities. Indeed, if the cavity is drastically overcoupled ($k \ll 1$) or undercoupled ($k \gg 1$), the cavity enhancement of the light is rather small, and high input powers will be needed to reach thermal nonlinearity. However, near critical coupling the cavity enhancement is optimal. Similarly, as FCA-induced heating depends on $ep \propto (2 \frac{k}{(1+k)^2}) \frac{Q_i}{V} P_{\text{in}}$ and FCD depends on $qp \propto (2 \frac{k^{3/2}}{(1+k)^{5/2}}) \frac{Q_i^{3/2}}{V} P_{\text{in}}$, the cavity enhancement is also optimal for the free-carrier effects near critical coupling.

B. Influence of V on p , ep , and qp

Additionally, we study the influence of the volume V of the cavity. The necessary scaling laws as a function of V were already derived in Sec. III A. However, the cavity in our paper is a microring, such that V is proportional to the round-trip length L of this microring. Therefore, we rephrase the previous scaling laws as a function of L .

In a microring with average waveguide loss $\alpha_{dB/m}$ (with bend loss included) and L not too large ($\ll 1/\alpha_{dB/m}$), $Q_i = \frac{2\pi n_g}{\alpha_{dB/m} \lambda_r} \frac{10}{\ln 10}$ is independent of L . However, a coupling section with power coupling K has $Q_c = \frac{\omega_r \tau_c}{2} = \frac{2\pi n_g L}{K \lambda_r}$, such that $k \propto L$ [15]. Furthermore, $V \propto L$. Hence, for a given $\alpha_{dB/m}$ and power coupling K , the cavity enhancement for both the thermal and free-carrier effects (to which, e.g., p , qp , and ep correspond) reaches an optimum at a value of L close to the one needed for critical coupling (i.e., $L_{\text{crit}} = \frac{K}{\alpha_{dB/m} \ln 10}$). However, if we optimize K for a given $\alpha_{dB/m}$ and L (such that k has a fixed value), the $1/V \propto 1/L$ dependence in the previous scaling laws for p , qp , and ep results in an improvement of the nonlinearity enhancement towards smaller L (provided the bend losses stay negligible). The critical coupling condition for rings with small L results in small K , which physically corresponds to larger gaps. This is an advantage, as this might circumvent the usage of racetrack resonators (with corresponding losses on the interface between rounded and straight waveguides) or the fabrication of rings with small gap features (which are difficult to process).

C. Influence of Q_i and k on q and e

Finally, given the scaling laws calculated in Sec. III A, we can also analyze how a changing cavity enhancement changes the relative importance of the corresponding different physical effects. This is reflected in the scaling laws of q and e . Indeed, as discussed in Sec. II, q expresses the relative importance of free-carrier generation versus heat generation by SSA.

Given $q \propto \frac{1}{\eta_{\text{lin}}} Q_i^{1/2} (\frac{1+k}{k})^{1/2}$, free-carrier effects will dominate in low-loss (high Q_i) cavities. Also, if $k \ll 1$, the light only stays in the cavity for a very short time, and in this limit the free-carrier effects dominate the heating due to linear absorption. Moreover, q decreases monotonically for increasing k and reaches a global minimum for $k \rightarrow \infty$. As $e \propto \frac{(1+k)}{k}$, similar conclusions are valid for the k dependence of e , representing the relative importance of the heating induced by FCA versus the heating induced by SSA.

IV. LINEAR STABILITY ANALYSIS

We now explain how the bistability, self-pulsation, and excitability regions can be calculated. In the next section we will then analyze how the different model parameters change the size of these regions.

The steady-state curves of Θ and N can be analytically calculated. Indeed, from Eqs. (9) and (10) it can be seen that $\Theta_{ss} = \frac{\sqrt{n_{ss}}}{q}(1 + ef n_{ss})$. Hence, at steady state

$$p = \frac{\sqrt{n_{ss}}}{q} \left[(1 + ef n_{ss})^2 + \left(\delta + \frac{\sqrt{n_{ss}}}{q}(1 + ef n_{ss}) - n_{ss} \right)^2 \right], \quad (11)$$

where $p(n_{ss})$ is a seventh-order polynomial in $\sqrt{n_{ss}}$, while $\Theta_{ss}(n_{ss})$ is a third-order polynomial. As $ef > 0$, Θ_{ss} is a monotonically increasing function of n_{ss} . Moreover, this steady state is independent of ϵ , i.e., the ratio between the free carrier and the thermal time scales.

We now substitute $\Theta(t) = \Theta_{ss} + \delta\Theta(t)$ and $n(t) = n_{ss} + \delta n(t)$ in Eqs. (9) and (10) and only retain the terms linear in $(\delta\Theta(t), \delta n(t))$. This results in a 2×2 Jacobian J_{ss} , with a quadratic characteristic equation:

$$\lambda^2 + \text{tr}(J_{ss})\lambda + \det(J_{ss}) = 0. \quad (12)$$

This equation has two roots, λ_1 and λ_2 . If $\det(J_{ss}) = 0$ and $\text{tr}(J_{ss}) \neq 0$, one of the roots will be 0 (a sign of a saddle-node bifurcation, resulting in bistability); if additionally $\text{tr}(J_{ss}) = 0$,

both roots are 0. If $\det(J_{ss}) > 0$ and $\text{tr}(J_{ss}) = 0$, both roots are purely imaginary, with $\lambda_2 = \lambda_1^*$ (a sign of a Hopf bifurcation). By substituting both $p(n_{ss})$ and $\Theta(n_{ss})$ into $\det(J_{ss})$ and $\text{tr}(J_{ss})$, $\det(J_{ss}) = 0$ and $\text{tr}(J_{ss}) = 0$ result in two sixth-order polynomial equations as a function of $\sqrt{n_{ss}}$. Hence, the corresponding six roots can be numerically tracked. Of course, only the real, positive roots have a physical meaning.

From Eqs. (9) and (10) it can be inferred that the only ϵ dependence of $\det(J_{ss})$ is a global $\frac{1}{\epsilon}$ scaling factor. Hence, as can be expected from Eq. (11), the solutions of $\det(J_{ss}) = 0$ are ϵ independent. This implies that the saddle-node bifurcation, i.e., the bistability onset, is also ϵ independent. However, the roots of $\text{tr}(J_{ss}) = 0$ are ϵ dependent. This implies that the Hopf bifurcation does depend on ϵ , and a good ϵ setting is therefore crucial in obtaining self-pulsation.

Using PYDSTOOL as numerical continuation software [10], starting from the Hopf bifurcations, we perform a limit-cycle continuation. That is, we track the change in limit-cycle shape caused by sweeping a certain parameter. Figure 3 illustrates for both $\delta = 0.5$ and $\delta = -3$ how the previously mentioned mathematical and numerical tools not only allow the calculation of the steady-state response of n_{ss} for fixed δ and changing p but also help to indicate the stability regions and to calculate the extreme values of n_{ss} corresponding to the branch of limit cycles originating from the Hopf bifurcation. While for $\delta = -3$ the curve is bistable, in the $\delta = 0.5$ case it is not. Moreover, for $\delta = 0.5$ the Hopf bifurcation is subcritical (i.e., nearby, a stable fixed point coexists with a surrounding unstable limit cycle), while for $\delta = -3$ the Hopf bifurcation is supercritical (i.e., nearby, an unstable fixed point coexists with a surrounding stable limit cycle).

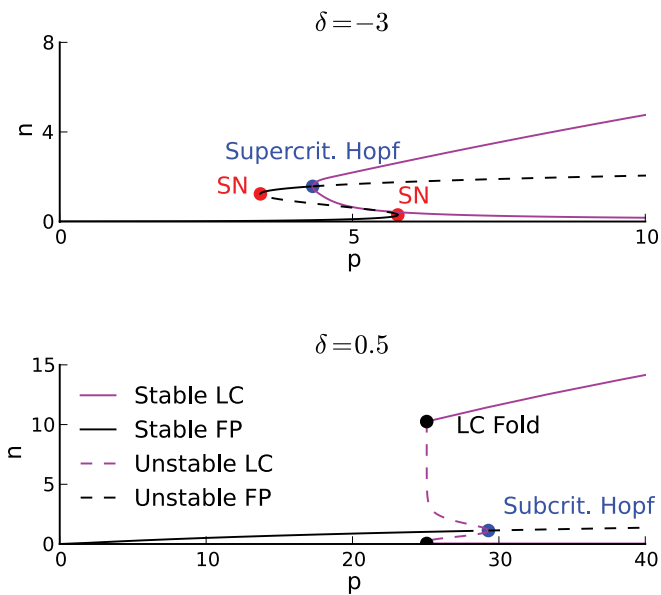


FIG. 3. (Color online) The steady-state response at $\delta = -3$ is, in between two saddle-node (SN) bifurcations, bistable and also has a supercritical Hopf bifurcation. At $\delta = 0.5$ no bistability is present, but an unstable limit-cycle branch (LC) originates from a subcritical Hopf-bifurcation and annihilates with a stable limit cycle branch in a limit-cycle fold (LC fold). To visualize the limit cycles, both the minimum and maximum values of the cycles are plotted. Stable and unstable fixed points (FP) or limit cycles are indicated with solid or dashed lines, respectively.

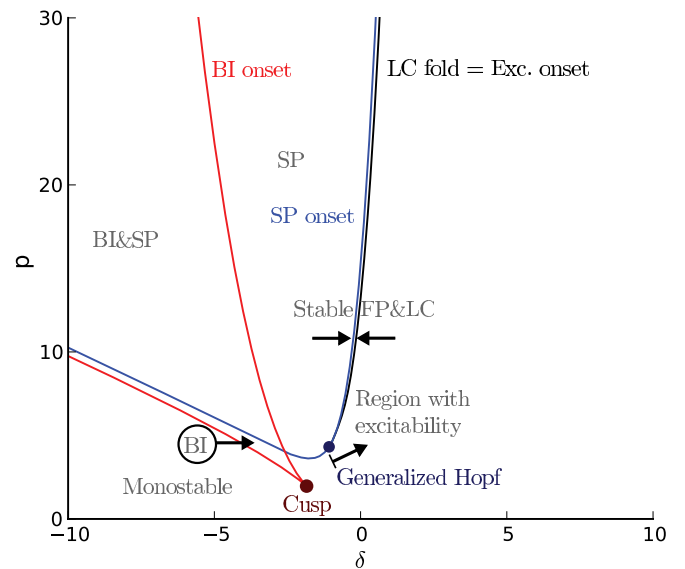


FIG. 4. (Color online) By tracking both the saddle-node bifurcations (BI onset) and Hopf bifurcation (SP onset) in the (δ, p) plane we can determine the bistability (BI) and self-pulsation (SP) region, respectively, which partly overlap (BI&SP). An LC fold branch originates from a generalized Hopf bifurcation on the self-pulsation onset curve such that for higher δ values excitability is present if p is below, but sufficiently close, to this LC fold branch. In between the self-pulsation onset and limit-cycle fold a stable fixed point coexists with an unstable limit cycle, surrounded by a stable one (stable FP&LC).

The subcritical Hopf bifurcation at $\delta = 0.5$ implies that, for lower input powers, the ring is excitable (Fig. 1, right). For a given cavity, the only free variables are the detuning δ and the input power p . In the (δ, p) plane (Fig. 4), the bistability (BI) onset disappears in a cusp bifurcation, while the Hopf bifurcation transits at a generalized Hopf (GH) bifurcation from supercritical ($\delta < \delta_{GH}$) to subcritical ($\delta > \delta_{GH}$). Hence, a fold bifurcation of a limit-cycle curve starts from a generalized Hopf bifurcation ($\delta_{GH} = -1.077, p_{GH} = 4.317$), towards $\delta > \delta_{GH}$. Subsequently, for $\delta > \delta_{GH}$ and sufficiently large p , but still smaller than the limit-cycle fold curve, the microring is excitable. The subcritical region of the Hopf bifurcation is mainly centered at the blue side ($\delta > 0$) of the resonance. This explains why excitability has until now only been measured in this wavelength region [4–6], instead of at the red side ($\delta < 0$) of the resonance.

V. INFLUENCE OF MODEL PARAMETERS ON BISTABILITY, SELF-PULSATION, AND EXCITABILITY

In Sec. III, we analyzed how optimizing the volume, the loss, and coupling of a cavity can reduce the required input power needed for nonlinear behavior and additionally changes the relative importance of the different physical effects (e.g., by changing q). In this section, we will investigate the influence of a change in q , ϵ , τ_{fc} , and f on the cavity dynamics in the (δ, p) plane or the (δ, n) plane.

A. Influence of q : FCD versus SSA

Whereas the bistability region only shifts slightly for changing $q = \frac{P_0^{ph}}{P_0^{el}}$ (as the bistability is mainly caused by the

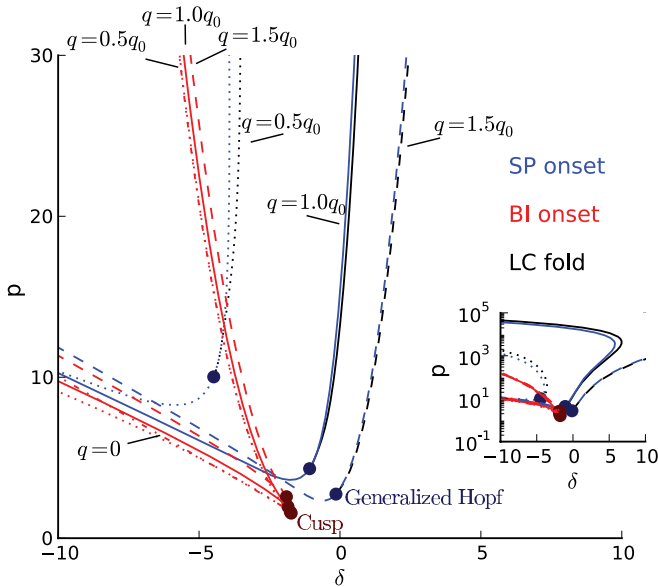


FIG. 5. (Color online) While the bistability region is only slightly dependent on the exact q value, the self-pulsation region and the corresponding excitability region shift clearly to higher δ for increasing q . The calculation was done for $q = 0.5q_0$ (dotted line), $q = q_0$ (solid line), and $q = 1.5q_0$ (dashed line), with $q_0 = 0.397$, i.e., the value from Fig. 1. For reference we also included the bistability curve for $q = 0$ (dash-dotted line), i.e., without any free-carrier effects.

thermal nonlinearity and, consequently, is rather insensitive for moderate changes in P_0^{el}), it should not be surprising that the self-pulsation region (and corresponding excitability onset) is heavily dependent on q (as they are caused by the interplay between thermal and free-carrier nonlinearities). We verify this in Fig. 5, for different q values, all with a predominant thermal nonlinearity (i.e., $q < 1$). A higher q value implies a shift of the self-pulsation region towards higher δ , such that the excitability region stops coinciding with the bistability region. As discussed in Sec. III, q can be changed by changing the cavity design. In principle, for $q = 0.5q_0$ (with $q_0 = 0.397$) we expect excitability at the red side of the resonance. However, the region is rather small and coincides with the bistability region. Hence, it will not be trivial to detect this experimentally. For $q = 0$, both the self-pulsation and excitability regions disappear, as in this case only the thermal nonlinearity is present.

B. Influence of time scale ratio ϵ

Slightly adapting the analysis method proposed in [7,8] to Eqs. (9) and (10), the influence of ϵ on the self-pulsation (SP) and bistability (BI) regions can be analyzed. We illustrate the calculation method together with some relevant definitions for $\delta = -3$ (where a generalized Hopf bifurcation appears) and $\delta = 0.5$ (in which case the Hopf bifurcation is always subcritical) in Fig. 6 and summarize the most interesting results in the (ϵ, δ) plane in Fig. 7.

We start by calculating the “on” and the “off” free-carrier detunings for self-pulsation ($n_{H,-}$ and $n_{H,+}$, respectively) and bistability ($n_{b,-}$ and $n_{b,+}$, respectively). Note that $n_{H,-/+}$ can be found by solving $\text{tr}[J_{ss}(p = p(n))] = 0$, while $n_{b,-/+}$ can be found by solving $\det[J_{ss}(p = p(n))] = 0$ (Sec. IV).

Furthermore, for a given δ , self-pulsation is only possible below a critical value ϵ_{sp} . The curve $(\epsilon_{sp}, \delta_{sp})$ can be calculated

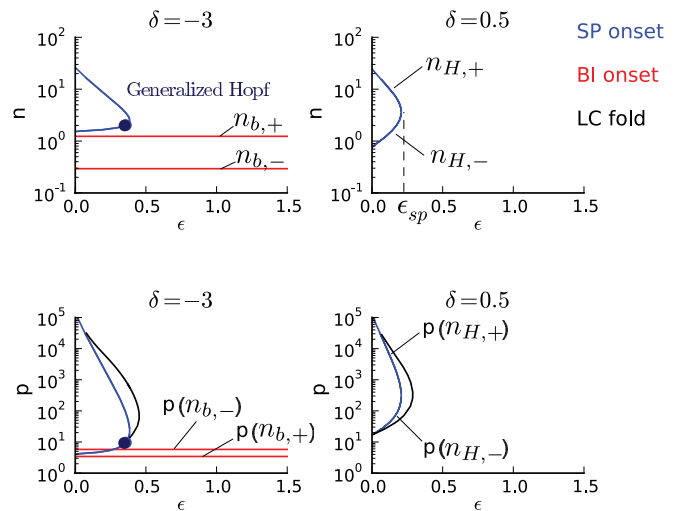


FIG. 6. (Color online) While the bistability region is independent of ϵ (with $q = 0.397$ fixed), the self-pulsation region becomes larger for smaller ϵ . For $\delta = -3$ a generalized Hopf bifurcation is present, while this is not the case for $\delta = 0.5$, as the Hopf bifurcation is then always subcritical. Self-pulsation appears in between $n_{H,-/+}$ [SP onset, blue (dark gray) lines], while bistability appears in between $n_{b,-/+}$ [BI onset, red (medium gray) lines]. For a given δ , self-pulsation is only possible below a critical value ϵ_{sp} . As before, LC fold (black line) reveals the excitability regions.

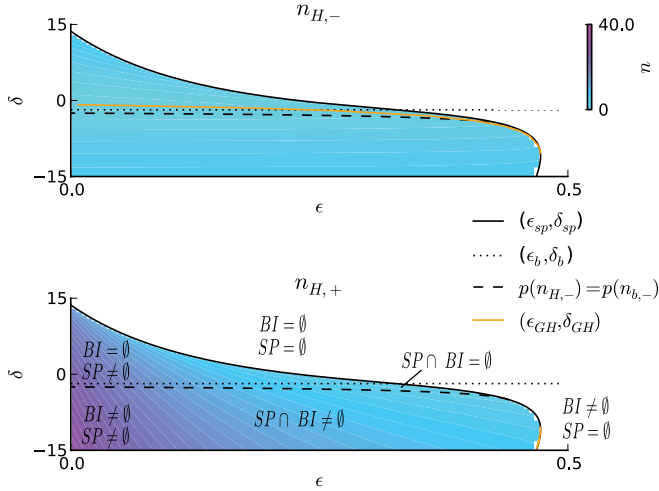


FIG. 7. (Color online) Summary of the regions with SP and BI in the (ϵ, δ) plane. The color levels represent the ‘on’ free-carrier detuning $n_{H,-}$ and the ‘off’ free-carrier detuning $n_{H,+}$ (with $q = 0.397$ fixed; definitions illustrated in Fig. 6). Here $(\epsilon_{sp}, \delta_{sp})$ encloses the region where some input powers result in self-pulsation (solid line); similarly, (ϵ_b, δ_b) encloses the region with bistability (dotted line). Furthermore, the curve $p(n_{H,-}) = p(n_{b,-})$ (dashed line) divides the region with bistability into a domain where $BI \cap SP = \emptyset$, where self-pulsation sets in only for powers above the bistable knee for up-switching, and a domain where $BI \cap SP \neq \emptyset$, where self-pulsation is present at the upper branch of the bistability curve. Finally, the generalized Hopf bifurcation location $(\epsilon_{GH}, \delta_{GH})$ on the $n_{H,-/+}$ surfaces is tracked [orange (light gray) line], indicating excitability is mainly present at the blue side of the resonance.

by tracking the fold bifurcation of $\text{tr}[J_{ss}(p = p(n))] = 0$ (using PYDSTOOL). Similarly (ϵ_b, δ_b) encloses the region with bistability ($BI \neq \emptyset$). In this case, δ_b is ϵ independent and thus needs to be calculated only once (using PYDSTOOL). Finally, the curve $p(n_{H,-}) = p(n_{b,-})$ divides the region where $BI \neq \emptyset$ into a domain where $BI \cap SP = \emptyset$, where self-pulsation sets in only for powers above the bistable knee for up-switching, and a domain where $BI \cap SP \neq \emptyset$, where self-pulsation is present at the upper branch of the bistability curve. $p(n_{H,-}) = p(n_{b,-})$ can be parameterized by, for a given δ , first solving $\det[J_{ss}(p = p(n))] = 0$ for $n_{b,-}$, subsequently solving $p(n_{H,-}) = p(n_{b,-})$ for $n_{H,-}$ (both calculations are ϵ independent; see Sec. IV), and finally solving $\text{tr}[J_{ss}(n = n_{H,-})] = 0$ for ϵ (a linear equation in ϵ).

The time scale ratio ϵ has no influence on the bistability region but severely influences the self-pulsation region (Figs. 6 and 7). If $\epsilon \rightarrow 0$, this region becomes larger. This illustrates how the difference in time scale between thermal and free-carrier relaxation is necessary for self-pulsation to occur. However, the presence of self-pulsation at $\epsilon = 0$ might seem unusual as self-pulsation can only occur in a system which is at least two-dimensional [16]. Indeed, if $\epsilon = 0$, one expects the system to be one-dimensional, as n changes its value instantaneously for a given $\Theta(t)$, such that $\frac{dn}{d\tau} = 0$ is satisfied. Nevertheless, the nullclines ($\frac{dn}{d\tau} = 0, \frac{d\Theta}{d\tau} = 0$) are independent of ϵ , and $\frac{dn}{d\tau} = 0$ results in a bistable relationship of n as a function of $\Theta(t)$ (Fig. 2); consequently, even at $\epsilon = 0$ the system still needs to be considered as two-dimensional. For

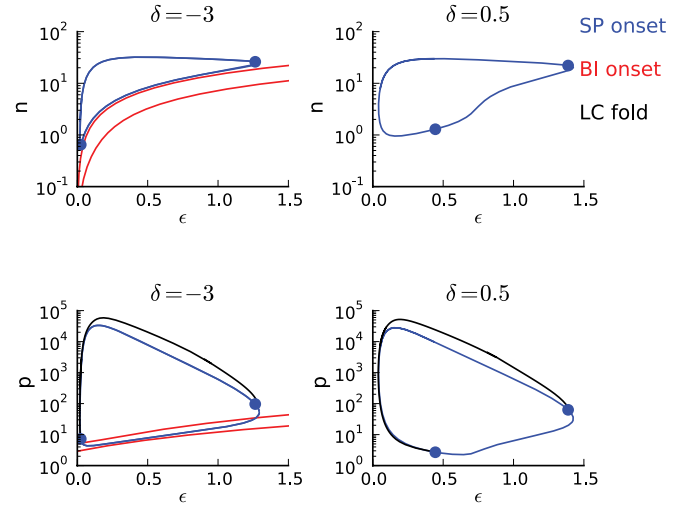


FIG. 8. (Color online) If $\epsilon = \frac{\tau_{fc}}{\tau_{th}}$ is changed by tweaking τ_{fc} , $q \propto \sqrt{\epsilon}$ due to $q \propto \sqrt{\tau_{fc}}$. Consequently, the decreasing q for $\epsilon \rightarrow 0$ causes the self-pulsation region to disappear (e.g., $\delta = -3$ and $\delta = 0.5$).

$\epsilon \rightarrow 0$, the transitions between the upper and lower branches of $\frac{dn}{d\tau} = 0$ will go infinitely fast, and Θ will stay fixed during these transitions. The dynamics at this limit thus deviate from the corresponding limit in nanocavities with a noninstantaneous Kerr effect [7].

In this paper, besides the self-pulsation onset, we are also interested in the excitability threshold (as opposed to [7,8], where the analysis only focused on the onsets of self-pulsation and bistability of a cavity without thermal heating effects). Therefore, we track the generalized Hopf bifurcation on the $n_{H,-/+}$ surfaces as this encloses the region where excitability will appear [Fig. 7, orange (light gray) lines]. Above $\delta \approx -10.44$ the $(\epsilon_{GH}, \delta_{GH})$ curve makes a transition from the $n_{H,+}$ surface to the $n_{H,-}$ surface, and the presence of this curve on the $n_{H,-}$ surface encloses the excitability region. If, for a given ϵ , δ is bigger than $\delta_{GH}(\epsilon)$, the (lower) onset of the self-pulsation region is a subcritical Hopf bifurcation, which implies that for input powers slightly lower than the self-pulsation onset the cavity will be excitable. From Fig. 7 it can be inferred that the subcritical Hopf bifurcation region on the $n_{H,-}$ surface is mainly centered at the blue side (i.e., $\delta > 0$) of the resonance, which confirms that excitability will mainly appear at the blue side of the resonance.

C. Influence of free-carrier lifetime τ_{fc}

The most straightforward manner to change $\epsilon = \frac{\tau_{fc}}{\tau_{th}}$ is by tweaking τ_{fc} . In a microring, this can, e.g., be done by reverse biasing a p - i - n diode over the waveguides [17] or by ion implantation [18]. However, as $q \propto \sqrt{\tau_{fc}}$, reducing τ_{fc} also reduces the strength of the free-carrier nonlinearities. We analyze this for two typical detuning cases ($\delta = -3$ and $\delta = 0.5$) in Fig. 8 and summarize the results in the (ϵ, δ) plane in Fig. 9. In contrast to Figs. 6 and 7, due to $q \propto \sqrt{\tau_{fc}}$ and $\epsilon \propto \tau_{fc}$, q is not fixed any longer but is proportional to $\sqrt{\epsilon}$. Moreover, we do not explicitly include $(\epsilon_{sp}, \delta_{sp})$ and $p(n_{H,-}) = p(n_{b,-})$ in Fig. 9 as the calculation is severely complicated by the $q(\epsilon \propto \tau_{fc})$ dependence.

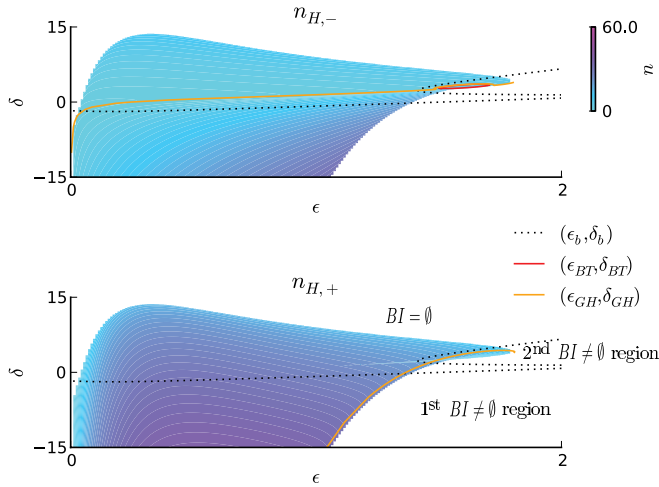


FIG. 9. (Color online) If $q = q_0 \sqrt{\frac{\epsilon}{\epsilon_0}}$ (q_0, ϵ_0 are the values used in Fig. 1), the color levels of the on free-carrier detuning $n_{H,-}$ and the off free-carrier detuning $n_{H,+}$ change with respect to Fig. 7, such that the self-pulsation region now disappears for $\epsilon \rightarrow 0$. For lower δ the self-pulsation region comes closer to $\epsilon = 0$; e.g., at $\delta = -15$ the self-pulsation region disappears at $\epsilon \approx 1.5 \times 10^{-3}$. Moreover, δ_b is now slightly ϵ dependent (dotted line). Additionally, a second bistability region appears for $\epsilon > 1.4$ near $\delta \approx 2.4$, which results in BT bifurcations [red (medium gray) line] when $n_{b,+}$ intersects with $n_{H,-}$.

As can be expected from Fig. 5, if $\tau_{fc} \rightarrow 0$, the self-pulsation region disappears. We remark that in this $\tau_{fc} \rightarrow 0$ limit, as soon as $\tau_{fc} \lesssim \tau_{ph}$, the fast light dynamics cannot be neglected any longer, and the model without approximation should be used. Additionally, not only is the bistability region corresponding to the one shown in Fig. 7 now dependent on τ_{fc} (and thus on ϵ), but also, due to stronger FCD, an additional bistability region appears for $\epsilon > 1.4$ near $\delta \approx 2.4$. The bistability onset $n_{b,+}$ of the latter region intersects with the self-pulsation onset $n_{H,-}$ in a Bogdanov-Takens bifurcation [BT, red (medium gray) line in Fig. 9]. Such a Bogdanov-Takens bifurcation will change the nearby cavity dynamics, as it often indicates a transition from “resonator” (class II) excitability to “integrator” (class I) excitability [16]. Finally, similar to Fig. 7, above the $(\epsilon_{GH}, \delta_{GH})$ curve on the $n_{H,-}$ surface [orange (light gray) line in Fig. 9] the self-pulsation onset is a subcritical Hopf bifurcation, which implies the presence of excitability for well-chosen input powers.

Another manner of changing ϵ , one we will not discuss in this paper, is to drastically change the ambient temperature of the chip, which will change both τ_{fc} and τ_{th} . Indeed, cryogenic experiments of SOI ring resonators show that the time scales of the thermal and free-carrier effects change in an opposite direction with decreasing temperature [19].

D. Influence of f : FCA versus FCD

Although we already incorporated FCA in the previous calculations ($f \neq 0$ and $e \neq 0$), we have not yet discussed in detail its influence as we used a fixed f value. As can be seen from Eq. (7), this value is mainly determined by the choice of material system. In SOI, the high q value, in combination with a high ef value, makes it impossible to neglect FCA in

our microring. If we were to neglect FCA ($f = 0$), or more precisely neglect the extra heating induced by FCA ($e = 0$), this would drastically change the steady-state solutions and the corresponding stability regions. Indeed, it can be calculated that both the self-pulsation region and the bistability region are then mainly centered at the blue side of the resonance (which can be partly understood from an analog situation in Fig. 9, where a high ϵ value, and thus, by the $\sqrt{\epsilon}$ proportionality, a higher q value, enhances FCD and results indeed in an extra bistability region at the blue side of the resonance). The ring is still excitable but in different (δ, p) regions. Moreover, as the self-pulsation region now overlaps with the bistability region, similar to the high ϵ region in Fig. 9, new bifurcations appear, such as a saddle-node homoclinic bifurcation, which change the nearby dynamics. Consequently, if $f \neq 0$ and $e \neq 0$, it is mainly the FCA-induced heating that causes the bistability region to be less dependent on the presence of free carriers (Fig. 5). Indeed, due to this additional heating the blueshift by FCD is partly compensated by a thermal redshift by the FCA-induced heating. Other theoretical studies confirm the importance of FCA in SOI cavities [8,9]. Given this significant influence of FCA in SOI, it might be interesting to analyze the nonlinear dynamics in material systems with a different FCA strength.

VI. CONCLUSION

A microcavity with both thermal and free-carrier nonlinearities self-pulsates or is excitable for certain power and wavelength settings of the input light. The required input power of the cavity decreases if the cavity is near critical coupling. If the fast light dynamics (buildup time of the cavity light) are neglected, the approximate boundaries of the regions in which this dynamic behavior is present can be calculated analytically. Free-carrier effects become more important if the linear loss of the cavity decreases, which increases the intrinsic Q factor Q_i . A higher Q_i increases the ratio of the characteristic nonlinear powers $q = \frac{P_0^{th}}{P_0^{ci}}$, which results in a shift of both the self-pulsation region and the excitability region towards higher detunings (i.e., towards the blue side of the resonance). High Q_i cavities are therefore needed to obtain this kind of dynamic behavior for low input powers. Additionally, in the case of microrings, we predict an optimal cavity enhancement of the nonlinearities for low-loss rings with a small round-trip length (but still not suffering from additional bend loss). Moreover, the self-pulsation region heavily depends on the time scale ratio $\epsilon = \frac{\tau_{fc}}{\tau_{th}}$, as the size of this region increases if $\epsilon \rightarrow 0$. However, in a realistic cavity a decrease in ϵ , e.g., by a decrease in the free-carrier lifetime τ_{fc} , implies a corresponding decrease in q . Indeed, $q \propto \sqrt{\tau_{fc}}$. Consequently, if $\tau_{fc} \rightarrow 0$, the self-pulsation region disappears. Given this trade-off, to enhance excitability and self-pulsation, τ_{fc} needs to be small, but nonzero, compared to the thermal lifetime τ_{th} .

ACKNOWLEDGMENTS

This work is supported by the interuniversity attraction pole (IAP) Photonics@be of the Belgian Science Policy Office and the ERC NaResCo Starting grant. T.V.V. is supported by the

TABLE I. Description and formula of the model parameters and, if appropriate, their (default) value.

Name	Description	Formula	Value
p	normalized input power	$P_{\text{in}}/(P_0^{\text{th}} \frac{1+k}{2})$	
δ	normalized detuning of the input light	$(\omega - \omega_r)\tau_{\text{ph}}$	
q	ratio thermo-optic shift (due to SSA-induced heating) to FCD	$\frac{P_0^{\text{th}}}{P_0^{\text{el}}}$	0.397
ϵ	time-scale ratio of the thermal effects to the free-carrier effects	$\frac{\tau_{fc}}{\tau_{\text{th}}}$	0.0815
e	related to FCA-induced heating	$\frac{1+k}{k\eta_{\text{lin}}}$	5
f	ratio of FCA to FCD	Eq. (7)	0.0714
k	fraction of good loading to losses	$\frac{\tau_c}{\tau_l}$	1
P_0^{th}	thermal characteristic intrinsic power (related to SSA)	Eq. (5)	$320 \mu\text{W}$
P_0^{el}	free-carrier characteristic intrinsic power (related to FCD)	Eq. (6)	$804 \mu\text{W}$
Q	loaded quality factor	$\frac{\omega_r \tau_{\text{ph}}}{2} = Q_l k / (1+k)$	6.25×10^4
τ_{ph}	photon lifetime	$(\tau_l^{-1} + \tau_c^{-1})^{-1}$	103 ps
τ_{th}	thermal relaxation time		65 ns
τ_{fc}	free-carrier relaxation time		5.3 ns

Flemish Research Foundation (FWO-Vlaanderen) by a Ph.D. grant. M.F. acknowledges the Special Research Fund of Ghent University. T.V.V. thanks PyDSTool developers R. Clewley and M. D. LaMar for their fast and accurate response to his questions.

APPENDIX: OVERVIEW OF THE MODEL PARAMETERS

In Table I, we summarize the definitions of the model parameters used in this paper. The default values are based on the SOI all-pass ring described in [4].

-
- [1] G. Priem, P. Dumon, W. Bogaerts, D. Van Thourhout, G. Morthier, and R. Baets, *Opt. Express* **13**, 9623 (2005).
- [2] W. H. P. Pernice, M. Li, and H. X. Tang, *Opt. Express* **18**, 18438 (2010).
- [3] T. J. Johnson, M. Borselli, and O. Painter, *Opt. Express* **14**, 817 (2006).
- [4] T. Van Vaerenbergh, M. Fiers, P. Mechet, T. Spuesens, R. Kumar, G. Morthier, B. Schrauwen, J. Dambre, and P. Bienstman, *Opt. Express* **20**, 20292 (2012).
- [5] M. Brunstein, A. M. Yacomotti, I. Sagnes, F. Raineri, L. Bigot, and A. Levenson, *Phys. Rev. A* **85**, 031803 (2012).
- [6] A. M. Yacomotti, P. Monnier, F. Raineri, B. Ben Bakir, C. Seassal, R. Raj, and J. A. Levenson, *Phys. Rev. Lett.* **97**, 143904 (2006).
- [7] A. Armaroli, S. Malaguti, G. Bellanca, S. Trillo, A. de Rossi, and S. Combrié, *Phys. Rev. A* **84**, 053816 (2011).
- [8] S. Malaguti, G. Bellanca, A. de Rossi, S. Combrié, and S. Trillo, *Phys. Rev. A* **83**, 051802 (2011).
- [9] S. Chen, L. Zhang, Y. Fei, and T. Cao, *Opt. Express* **20**, 7454 (2012).
- [10] R. H. Clewley, W. E. Sherwood, M. D. LaMar, and J. M. Guckenhaimer, PYDSTOOL, a software environment for dynamical systems modeling, 2007, <http://pydstool.sourceforge.net/>.
- [11] M. Fiers, T. Van Vaerenbergh, K. Caluwaerts, D. V. Ginste, B. Schrauwen, J. Dambre, and P. Bienstman, *J. Opt. Soc. Am. B* **29**, 896 (2011).
- [12] CAPHE, <http://www.caphesim.com>.
- [13] M. Soljačić, M. Ibanescu, S. G. Johnson, Y. Fink, and J. D. Joannopoulos, *Phys. Rev. E* **66**, 055601 (2002).
- [14] P. Barclay, K. Srinivasan, and O. Painter, *Opt. Express* **13**, 801 (2005).
- [15] A change in round-trip length L can, of course, imply a change in the curvature at the coupling section (reflected in a change in K), but this is an indirect dependence, which is not important for the current reasoning.
- [16] E. M. Izhikevich, *Dynamical Systems in Neuroscience: The Geometry of Excitability and Bursting*, Computational Neuroscience Series (MIT Press, Cambridge, MA, 2006).
- [17] A. C. Turner-Foster, M. A. Foster, J. S. Levy, C. B. Poitras, R. Salem, A. L. Gaeta, and M. Lipson, *Opt. Express* **18**, 3582 (2010).
- [18] M. Waldow, T. Plötzing, M. Gottheil, M. Först, J. Bolten, T. Wahlbrink, and H. Kurz, *Opt. Express* **16**, 7693 (2008).
- [19] W. H. P. Pernice, C. Schuck, M. Li, and H. X. Tang, *Opt. Express* **19**, 3290 (2011).